Drug Design, Development and Therapy

Dovepress
Taylor & Francis Group

Open Access Full Text Article

ORIGINAL RESEARCH

Modified Huanjingjian Prevents Chemotherapy-Induced Alopecia by Inhibiting Genomic DNA Methylation of the Wnt Signaling Pathway in Mice

Xin Liu[1,*], Ting Du[1,*], Ruofan Xi[1,*], Linyan Cheng[1], Yi Wang[1], Hanzhi Lu[1], Dongjie Guo[1], Jianyong Zhu[2], Te Liu[3], Fulun Li[1]

[1]Department of Dermatology, Yueyang Hospital of Integrated Traditional Chinese and Western Medicine, Shanghai University of Traditional Chinese Medicine, Shanghai, 200437, People's Republic of China; [2]Department of Pharmacy Research, Yueyang Hospital of Integrated Traditional Chinese and Western Medicine, Shanghai University of Traditional Chinese Medicine, Shanghai, 200437, People's Republic of China; [3]Shanghai Geriatric Institute of Chinese Medicine, Shanghai University of Traditional Chinese Medicine, Shanghai, 200031, People's Republic of China

*These authors contributed equally to this work

Correspondence: Te Liu, Shanghai Geriatric Institute of Chinese Medicine, Shanghai University of Traditional Chinese Medicine, 365 South Xiangyang Road, Shanghai, 200031, People's Republic of China, Email liute1979@shutcm.edu.cn; Fulun Li, Department of Dermatology, Yueyang Hospital of Integrated Traditional Chinese and Western Medicine, Shanghai University of Traditional Chinese Medicine, 110 Ganhe Road, Shanghai, 200437, People's Republic of China, Email drlifulun@163.com

Aim: Cyclophosphamide (CTX), a cornerstone in breast cancer combination chemotherapy, frequently induces adverse effects including myelosuppression, gastrointestinal disturbances, hepatic impairment, and alopecia. Chemotherapy-induced alopecia severely impacts patients' quality of life and psychological well-being. Modified Huanjingjian (MHJJ), a traditional Chinese herbal formula, demonstrates clinical efficacy in alleviating chemotherapy-related side effects, yet its mechanisms against CTX-induced alopecia remain uncharacterized. And our main aim was to explore the efficacy and the mechanism of MHJJ in mice.

Methods: UPLC-QE-Orbitrap-MS characterized MHJJ's chemical composition. A CTX-induced alopecia murine model was established. Systemic toxicity was evaluated through body weight monitoring, automated biochemical analysis (ALT/AST levels), and hematological profiling (WBC/PLT counts). Hair follicle histopathology was assessed via H&E staining. IHC and IF staining quantified proliferation markers and hair follicle stem cell (HFSC) biomarkers. Reduced representation bisulfite sequencing (RRBS) was used to map DNA methylation patterns. Wnt pathway dynamics were analyzed through qRT-PCR and IF staining.

Results: We identified 110 bioactive compounds in MHJJ. MHJJ intervention attenuated alopecia severity, restored follicular architecture, and increased follicular density compared to CTX monotherapy ($p<0.05$). HFSC proliferation markers (Ki67/CD34) showed significant upregulation, while apoptosis markers (Caspase-3) were suppressed. RRBS revealed MHJJ-mediated hypomethylation in differentially methylated regions, with gene body methylation constituting 60% of total methylation changes. Methylation-modulated genes predominantly localized to Wnt signaling pathways: MHJJ enhanced Wnt3/Wnt10a expression while suppressing Cer1/Axin1. Corresponding methylation reductions at promoter and gene body regions were confirmed at mRNA and protein levels.

Conclusion: MHJJ mitigates CTX-induced alopecia through epigenetic regulation of HFSCs, specifically via DNA hypomethylation-mediated activation of Wnt3/Wnt10a and suppression of Cer1/Axin1. This mechanism promotes follicular regeneration by restoring Wnt signaling homeostasis, positioning MHJJ as a promising adjuvant for chemotherapy-induced alopecia management.

Keywords: traditional Chinese medicine, chemotherapy-induced alopecia, hair follicle, DNA methylation, Wnt signaling pathway

Introduction

Cyclophosphamide (CTX) is often an important component of combination chemotherapy regimens in the treatment of breast cancer.[1] CTX inhibits the proliferation of cancer cells by cross-linking and damaging the DNA of the breast cancer

Received: 11 March 2025
Accepted: 24 June 2025
Published: 11 July 2025

Graphical Abstract

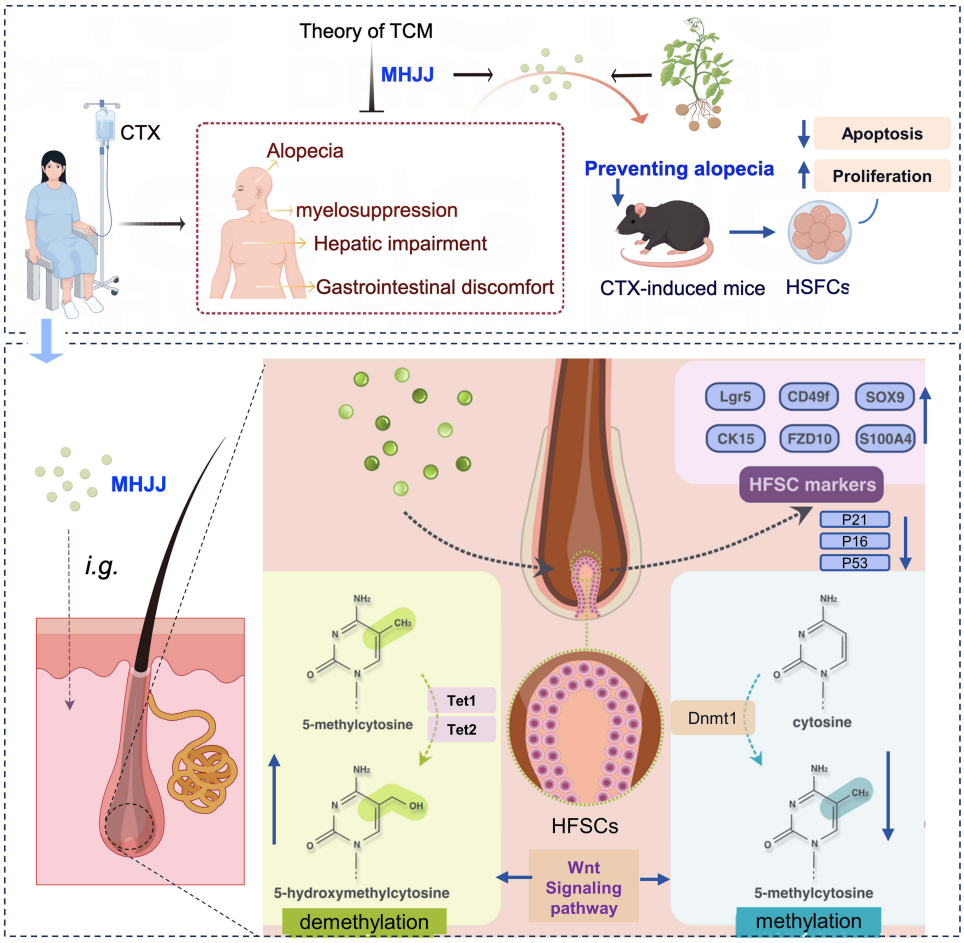

cells through its alkylating effect.[2] However, CTX is inhibitory to all cells that proliferate significantly, and it damages healthy cells including HFSCs.[3] HFSCs are considered to be the major stem cells involved in hair production. HFSCs divide rapidly, which makes chemotherapy even more damaging to them. As chemotherapy inhibits cell division in HFSCs, the circulation and regeneration of HFs is impaired and remains in the resting phase, ultimately leading to alopecia, with an estimated incidence of 65%.[4] There are better symptomatic clinical options for myelosuppression and gastrointestinal complaints caused by CTX chemotherapy. However, alopecia, which is a major concern for female patients, seriously affects their mental health, and there is no better way to prevent it. Scalp cooling therapy is a clinically recommended treatment, and the theory behind it is to constrict blood vessels near the hair follicles, so that chemotherapeutic drugs cannot reach these rapidly dividing cells. However, ice cap therapy can cause head coldness, headaches and is uncomfortable to wear. Ice caps are not entirely effective in preventing alopecia, and their end result often is thinning hair that remains aesthetically pleasing.[5] Therefore, going through the process of scalp cooling may not become worthwhile. There is an urgent need to develop new treatments to prevent cyclophosphamide-induced alopecia.

Chinese medicine believes that healthy qi is sufficient inside the body, pathogenic factors cannot invade.[6] Chemotherapeutic agents are considered strong pathological factors (referred to in Traditional Chinese Medicine as "harsh evils") that damage the body's healthy qi and disrupt internal balance. The imbalance is manifested as the impaired function of the spleen and stomach in absorbing nutrients, as well as the impaired functions of the liver in storing blood and the kidney in

storing essence, which are closely related to the growth, development, reproduction and other functions of the human body. One of the manifestations of liver - kidney deficiency is myelosuppression and alopecia.

Chinese medicine has been clinically and scientifically proven to be effective in the treatment of a wide range of diseases, including the adverse effects associated with antitumor drugs.[7,8] Patients who received TCM decoctions for jian pi (to regulate gastrointestinal function for better assimilation) and yi qi yang xue sheng sui (to enhance bone marrow hematopoietic activity) could lower the risk of severe chemotherapy - induced leukopenia, neutropenia, and febrile neutropenia in breast cancer patients.[9] Chinese medicinal herbs may cut therapeutic toxicity, clear heat, boost immunity, relieve fatigue, and have antineoplastic and anti-inflammatory effects, enhancing patients' ability to fight cancer.[8] By integrating herbal medicine with conventional chemotherapy, this combinatorial approach may synergistically enhance treatment efficacy while reducing chemotherapy-associated adverse events, such as nausea/vomiting, diarrhea, alopecia, myelosuppression, and immune dysfunction, thereby improving patients' resilience during oncological treatment.[10–12]

Our study focuses on a TCM formulation, MHJJ, which is an Hospital - prepared Medicines (Record No.: Shanghai Pharmaceutical Preparation Zi: Z20200024000), and has been widely used in breast cancer patients with TCM evidence of liver - kidney deficiency. MHJJ consists of 9 herbs, Cuscutae semen, Astragali complanati semen, Lycii fructus, Ligustri lucidi fructus, Mori fructus, Longan arillus, Poria, Astragali radix, Crataegi fructus. Among them, Cuscutae semen, Lycii fructus, as the monarch, both tonifying the kidney essence; Astragali complanati semen sweet warm, tonifying the kidney essence for the subject; Lycii fructus, Mori fructus, Ligustri lucidi fructus tonifying the kidney nourishing yin, nourishing the liver and tonifying the blood as the subject of the medicine; supporting the Astragali radix to tonify the qi, blood, hair; Longan arillus, Poria benefit the heart qi, tranquillising the spirit of the drug; Crataegi fructus spleen and food, and eliminate blood stasis as a total of medicinal drugs, and the above five children match, tonic with a diarrhoea, complementary and not greasy.

Among the components of MHJJ, Lycii fructus, Poria and Longan arillus are frequently consumed in daily diet and medicinal diet, and they have anti-tumor, anti-oxidation, hypoglycemic, lipolytic and heart-protective effects.[13] Lycium barbarum polysaccharides showed immunomodulatory activity in cyclophosphamide CTX-treated mice by restoring the damaged immune organs and adjusting the T lymphocyte subsets.[14] Study shows medium/high-dose Ligustri Lucidi Fructus increases WBC and bone marrow nucleated cell counts, adjusts thymic/splenic indices, and inhibits Caspase-3 expression.[15] Astragalus mongholicus and Semen Cuscutae can improve chemotherapy-induced leukopenia.[16] Lycium barbarum polysaccharide attenuates chemotherapy-induced ovarian injury by reducing oxidative stress.[17] Crataegi fructus contains a variety of fruit acids, several studies have shown that Ursolic acid and Oleanolic acid can reduce the risk of intestinal pathological injury, alleviate intestinal dysfunction, and restore intestinal barrier function.[18] Astragali complanati semen contains flavonoids, which may alleviate chemotherapy-related fatigue and bone marrow suppression through antioxidant and immunomodulation.[19] Mori fructus, Preclinical investigations demonstrate its broad-spectrum pharmacological properties encompassing antioxidant defense enhancement, neuroprotection, immunomodulation, antitumor, and metabolic regulation through glucose/lipid homeostasis modulation.[20] All of the above drugs are part of MHJJ, suggesting that MHJJ has the potential to treat the side effects of chemotherapy.

Similarly, the components of MHJJ demonstrate therapeutic potential for various alopecia subtypes. A botanical formulation containing Astragalus membranaceus and Ligustrum lucidum, has been shown to promote hair growth through upregulation of vascular endothelial growth factor (VEGF) expression.[21] Polysaccharides are considered to be the most important active substances in Lycii fructus,[22] Quercetin is an important component in Cuscutae semen, Mori fructus and Astragali complanati semen, It was found that topical delivery of quercetin stimulates resting hair follicles to grow with rapid follicular keratinocyte proliferation and replenishes perifollicular microvasculature in mice.[23]

Previous studies have noted that components from TCMs could treat certain diseases by regulating DNA methylation. Astragalus polysaccharides are reported to improve osteoporosis in mice through genomic DNA methylation regulation.[24] Poria cocos polysaccharides could alleviate chronic non-bacterial prostatitis by remodeling the DNA methylome.[25] A flavone compound, kaempferol, could reduce the downregulation of DNA methyltransferase DNMT3b in bladder cancer by regulating genomic methylation.[26] All the components mentioned above are also in the MHJJ formula. These observations support the hypothesis that the traditional Chinese medicine MHJJ exerts the

therapeutic effects on alopecia by regulating methylation levels and the differentially methylated genes are likely related to the Wnt signaling pathway.

TCM theory suggests that the main function of MHJJ is to tonify the kidney function and fill up the essence,[27] support the healthy qi and dispel the evil. When used prior to chemotherapy, it can significantly reduce myelosuppression, gastrointestinal discomfort and alopecia in patients.[8] Given that Chinese herbal compounds with similar efficacy to MHJJ are effective in preventing CTX-induced side effects in clinical applications,[28] we would like to further explore the pharmacodynamic basis for the prevention of CTX-induced alopecia by MHJJ.

Epigenetic dysregulation plays a role in autoimmune skin diseases such as alopecia, in which DNA modification including methylation and hydroxymethylation is involved.[29] DNA methylation is not only a normal and regular modification in eukaryotes but also a dominant epigenetic way to regulate gene expression in mammals. It happens when a methyl group combines with the 5-carbon of the cytosine by a covalent bond in a CpG dinucleotide of a genome with DNA methyltransferase.[30] DNA methylation has been validated in numerous studies to regulate gene expression by altering chromatin structure, DNA conformation and stability, and the way DNA interacts with proteins.[31] The promoter CpG islands (CGIs), the 5' non-coding region, or the first exon region of a gene are common DNA methylated sites.[32] DNA methylation is usually regarded as inhibiting gene transcription and downregulating its expression. It was reported that the DNA that coded androgen receptors in occipital HFs were hypermethylated in AGA.[33] The global DNA hypermethylation of the peripheral blood monocytes in patients with alopecia was observed, and the transcription level of DNA methyltransferase 1 (DNMT1) significantly increased.[34] As for DNMT1, evidence shows that it plays an important role in the renewal and differentiation of stem cell, and furthermore, maintaining its homeostasis in HFs.[35,36] The reports mentioned above have already revealed a close relationship between certain types of alopecia and DNA methylation; We sought to explore whether MHJJ prevents CTX-induced alopecia by modulating HFSCs gene methylation.

Materials and Methods

Preparation of MHJJ

The composition of MHJJ is listed in Table 1. The botanical drugs were provided by Yueyang Hospital of Integrated Traditional Chinese and Western Medicine and validated taxonomically. The herbs were soaked in 1000 mL water for 20 min. After heating the herbs and water to boiling, boil for another 30 min at 100 °C and filter out the decoction. Then another 1000 mL water was added to the herbs and boiled. The above procedure was repeated twice. Then the obtained decoctions were filtered and evaporated (pressure of 0.08 MPa and temperature of 60 °C) with a rotary evaporator (N-1300-WB, Tokyo Rikakikai Co., Ltd.) to remove its solvent to obtain a concentrated liquid with a relative density between 1.03–1.10. The obtained preparation was used as the high dose group, and the rest of the medium dose group and the low dose group were obtained by taking this dose and diluting it with saline in equal proportions. In the MHJJ group, each mouse was orally administered the MHJJ formula (200 μL/d). The MHJJ dosage was calculated as previously described.[37] The calculated dosage for mice was 9.09 mL/kg/d, which was approximately equal to 198 μL/d for each mouse. All the

Table 1 Botanical Drugs in the MHJJ Formula

Botanical Drugs	Source Plants	Family	Medicinal Part	Dose (g)
Cuscutae semen	*Cuscuta chinensis* Lam.	Convolvulaceae	Seed	40
Astragali complanati semen	*Phyllolobium chinense* Fisch.	Fabaceae	Seed	50
Lycii fructus	*Lycium barbarum* L.	Solanaceae	Fruit	40
Ligustri lucidi fructus	*Ligustrum lucidum* W.T.Aiton	Oleaceae	Fruit	40
Mori fructus	*Morus alba* L.	Moraceae	Fruit	36
Longan arillus	*Dimocarpus longan* Lour.	Sapindaceae	Aril	48
Poria	*Poria cocos* (Schw.) Wolf	Polyporaceae	Mycorrhizal nucleus	36
Astragali radix	*Astragalus membranaceus* (Fisch.) Bge. var. *mongholicus* (Bge.) Hsiao	Fabaceae	Root	60
Crataegi fructus	*Crataegus pinnatifida* var. Bge. *major* N.E.Br.	Rosaceae	Fruit	24

listed botanical drug were purchased from Shanghai Wanshicheng Pharmaceutical Co., Ltd. (Shanghai, China) with the following specifications: *Cuscutae semen* (Batch No. 230303); *Astragali complanati semen* (Batch No. 230105); *Lycii fructus* (Batch No. 230212); *Ligustri lucidi fructus* (Batch No. 230208); *Mori fructus* (Batch No. 230206); *Longan arillus* (Batch No. 230202); *Poria* (Batch No. 230315); *Astragali radix* (Batch No. 230318); *Crataegi fructus* (Batch No. 230320). All the above samples are stored in the Department of Pharmacy Research at the hospital.

Preparation of CTX Injection

Before administration, 1.5 g CTX (Sigma-Aldrich, 6055-19-2, MO, USA) was freshly dissolved in 10 mL saline (Yueyang Integrated Chinese and Western Medicine Hospital, Shanghai, China) to prepare a master mix. The solution was filtered through a 0.22 μm filter.

Ethics Statements

All animal experiments were carried out strictly in accordance with the Guideline for Ethical Review of Laboratory Animal Welfare of the General Administration of Quality Supervision, Inspection and Quarantine of the People's Republic of China. The protocol was approved by Institutional Animal Care and Use Committee (IACUC) at Yueyang Integrated Chinese and Western Medicine Hospital (Assurance Number YYLAC-2021-126). Mice were anaesthetised by inhalation of isoflurane and executed by an overdose of sodium pentobarbital.

Animal Experiments

Female C57BL/6 mice (6–8 weeks of age) were purchased from Shanghai Jihui Laboratory Animal Co., Ltd. (Shanghai, China) with a license numbered SYXK (Hu) 2018–0040. Study procedures involving animal subjects were reviewed and approved by the Institutional Animal Care and Use Committee of Yueyang Hospital of the Integrated Traditional Chinese and Western Medicine (No. 20170012026440034). Mice were bred in a normal facility (room temperature of 20 °C–26 °C, relative humidity of 40%–70%, and 12 h light/12 h dark cycle) and fed with normal diets. After 1 week of acclimation, 30 mice were randomly divided into 5 groups (n = 6 per group): control group (WT), CTX model group (CTX), and groups administrated with low dose of MHJJ (LOW), medium dose of MHJJ (MID) and high dose of MHJJ (HIGH). One mouse per group was used for preliminary experiments, leaving 5 mice per group (n = 5) for formal experiments. The grouping was blinded to the observers and researchers analyzing the data.

The experimental period lasted 49 days, with the timeline and interventions as follows: Days 1–21 (Preconditioning): WT and CTX groups received oral saline (200 μL/day). LOW, MID, and HIGH groups received MHJJ at the designated dose. Days 21–28 (CTX-induced damage phase): CTX and all MHJJ groups received CTX at 70 mg/kg/day intraperitoneally, alongside their original oral treatment. WT group continued with oral saline only. Day 29 (Hair depilation and baseline assessment): Mice were anesthetized using 4% isoflurane and the dorsal hair was removed with a 1:1 rosin/wax mixture. Photographs were taken to document baseline hair status. Days 29–49 (Hair regeneration phase): CTX and MHJJ groups received CTX at a maintenance dose of 7 mg/kg/day intraperitoneally. MHJJ oral treatments continued unchanged and WT group continued with oral saline only. On day 49, the body weight of mice was recorded. In the WT group, mice were given 0.9% NaCl sterile physiological saline (pH 7.2–7.4) orally throughout the treatment. Blood was then collected from the orbital venous plexus using a glass capillary while the mice were under anesthesia, Finally, the mice were sacrificed with an overdose of sodium pentobarbital, the back of the mice was photographed to record the hair condition, and skin tissue from the dorsal decidualised area of each mouse was immediately collected for subsequent experimental validation.

UPLC-QE-Orbitrap-MS for Component Analysis

The extract of MHJJ was diluted with methanol and centrifuged (13,000 rpm, 10 min). The supernatant was filtered through a 0.22 μm filter. Then the sample was subjected to ultra-performance liquid chromatography-quadrupole-electrostatic field orbitrap-tandem mass spectrometry (UPLC-QE-Orbitrap-MS) analysis to characterize the component. The UPLC-QE-Orbitrap-MS was archived on a Vanquish UPLC system (Thermo Fisher Scientific, MA, USA) with an Orbitrap Exploris 120 mass spectrometer (Thermo Fisher Scientific, MS, USA).

The chromatographic separation was conducted with an ACQUITY UPLC BEH C18 column (2.1 mm × 100 mm, 1.7 μm, Waters, MA, USA). The mobile phase was 0.1% formic acid aqueous solution (A) and 0.1% formic acid acetonitrile solution (B). The flow rate of the mobile phase was 0.3 mL/min, the column temperature was 35 °C, and the injection volume was 5 μL. The multi-step linear elution gradient program was as follows: 0–11 min, 85%–25% A; 11–12 min, 25%–2% A; 12–14 min, 2% A; 14–14.1 min, 2%–85%; 14.1–16 min, 85% A.

The MS/MS data were collected based on the information-dependent acquisition (IDA) mode. During each acquisition cycle, the *m/z* range was from 100 to 1500. The optimized parameters were as follows: sheath gas flow rate of 35 Arb, aux gas flow rate of 15 Arb, ion transfer tube temperature of 350 °C, vaporizer temperature of 350 °C, collision energy of 16/32/48 in NCE mode, spray voltage of 5.5 kV in positive mode and −4 kV in negative mode. The mass spectrometry data were collected and processed by Xcalibur software (Thermo Fisher Scientific, CA, USA).

Fully Automated Biochemical Analysis

Vacuum blood collection tubes containing an anticoagulant (EDTA) are used. Collect venous blood samples, centrifuge to separate serum or plasma, and check the samples for abnormalities such as haemolysis. Turn on the instrument to warm up, calibrate the instrument with calibrators, then perform quality control tests and start testing samples after passing the test. Select the test items via the operating software, set the wavelength, reagent dosage and other parameters. The sample and reagents are added to the reaction cup according to the procedure, and the chemical reaction takes place at a constant temperature of 37°C.

Blood Cell Analysis

Blood is collected in a blood collection tube containing an anticoagulant (EDTA), mixed thoroughly and diluted appropriately according to the requirements of the instrument. The diluted blood sample is put into the inlet of the blood cell analyser. The whole testing process is controlled by the built-in computer system of the instrument, which automatically completes the data collection, analysis and recording.

RNA Isolation and qRT-PCR

Total RNA was extracted using TRIzol (Thermo Fisher Scientific, CA, USA) from skin tissues. The RNA purity was detected using Nanodrop 1000 (Thermo Fisher Scientific, CA, USA). Total RNA was reverse transcribed to cDNA with M-MLV reverse transcriptase (Promega, Madison, USA) and ribonuclease inhibitor (Sigma-Aldrich, MO, USA). The qRT-PCR analysis was carried out with SYBR Green Real-time PCR Master Mix (Toyobo, Shanghai, China) and the CFX96 Touch Real-Time PCR detection system (Bio-Rad Laboratories, Inc., CA, USA) for a total of 40 cycles (95 °C for 15s, 58 °C for 30s, and 72 °C for 42s). The mRNA expression levels were calculated using the $2^{-\Delta\Delta CT}$ method, and 18SrRNA was selected as an internal reference gene. The sequences of primers are shown in the Supplementary Table 1.

H&E Staining

Skin histopathology morphology was examined using a H&E staining method. The protocol was similar to the one that was previously described. The slides were observed under a BX-51 microscopy (Olympus, Japan) and photographed by a DP-70 digital camera (Olympus, Japan). Photomicrographs were analyzed and the positive ratio was calculate using ImageJ software (v1.54).

IHC Staining

The expression of the proliferation marker Ki67 was assessed by immunohistochemistry. Briefly, 4 μm-thick paraffin-embedded skin sections were baked at 65 °C for 120 min, dewaxed in xylene, and rehydrated through a graded series of ethanol solutions. Following two washes in PBS (5 min each), antigen retrieval was performed in sodium citrate buffer (pH 6.0) by boiling for 20 min. After cooling to room temperature, sections were washed three times with PBS (5 min each) and then incubated with endogenous peroxidase blocking reagent at room temperature for 10 min. After additional PBS washes (3 × 5 min), sections were blocked with 5% BSA for 30 min at room temperature. The primary antibody against Ki67 (GB121141, Servicebio, Wuhan, China) was diluted in 5% BSA and applied to each section (approximately

100 μL) for overnight incubation at 4 °C. The next day, slides were brought to room temperature, washed in PBS (3 × 5 min), and incubated with the appropriate secondary antibody for 90 min. After washing (3 × 2 min), immunoreactivity was visualized using DAB substrate, followed by hematoxylin counterstaining. Sections were then dehydrated and mounted. Images were acquired under a light microscope, and the percentage of Ki67-positive cells was quantified using ImageJ software (v1.54, NIH, USA).

IF Staining

Skin tissues were fixed in 4% paraformaldehyde (Sigma-Aldrich, MO, USA) for 30 min at room temperature, followed by graded ethanol dehydration and paraffin embedding. Paraffin sections (6 μm thick) were dewaxed in xylene and rehydrated through a graded ethanol series. Sections were blocked with immunofluorescence (IF) blocking buffer (P228, Beyotime Biotechnology, Zhejiang, China) at 37 °C for 30 min, then washed three times with PBST (PBS containing 0.1% Tween-20) for 5 min each at room temperature. Subsequently, the sections were incubated at 37 °C for 45 min with primary antibodies diluted in IF blocking buffer. The primary antibodies included: Lgr5 (ab273092), CD49f (Integrin α6, ab181551), SOX9 (ab185966), S100A4 (ab93283), CK15 (ab52816), and FZD10 (ab137491) (all from Abcam, Cambridge, UK). After washing three times with PBST, sections were incubated with the appropriate fluorophore-conjugated secondary antibodies at 37 °C for 45 min in the dark. Finally, after another set of PBST washes (3 × 5 min), nuclei were counterstained with DAPI if required, and the sections were mounted with anti-fade mounting medium. Fluorescence images were captured using a fluorescence microscope (eg, Leica or Zeiss), and analyzed with ImageJ software (v1.54).

Reduced Representation Bisulfite Sequencing

The genomic DNA of skin tissues was digested with MspI, and the ends of MspI-digested DNA were repaired and dA-tailed. The bisulfite conversion of adaptor-ligated DNA was performed by using an EZ DNA Methylation Gold Kit (Zymo Research, CA, USA). After that, the bisulfite-treated DNA was PCR-amplificated. The library DNA concentration was analyzed by Qubit 2.0 (Thermo Fisher Scientific, CA, USA) and readjusted to 1 ng/μL. Afterward, the fragment size range and molarity of each library were checked with the Bioanalyzer 2100 (Agilent, CA, USA). The concentration of libraries was recalculated in accordance with the index ratios, and the full-scale sequencing was conducted on the HiSeq platform (Illumina, USA) after a sufficient pool of RRBS libraries for sequencing was prepared.

Functional Enrichment Analysis

The differential methylated genes then underwent functional analysis including Kyoto Encyclopedia of Genes and Genomes (KEGG) analysis and Gene Ontology (GO) enrichment analysis, encompassing BP (biological process), MF (molecular function), and CC (cellular component). The GO and KEGG analysis were performed via the Metascape database (https://www.metascape.org), with a minimum enrichment of 1.5, a minimum overlap of 3, and $P < 0.01$ as the threshold.

Data Analysis

All experiments were repeated for five independent trials. GraphPad Prism 8.0 (GraphPad Software, CA, USA) was applied for data analysis, and results were presented as mean ± standard deviation (SD). The significance between multiple sets of independent data was analyzed using one-way analysis of Variance (ANOVA) and Bonferroni post-hoc tests. Values of $P < 0.05$ were considered statistically significant.

Results

Main Components of MHJJ

In order to initially identify the types of compounds in MHJJ, we performed compositional identification using mass spectrometry analysis. A total of 243 compounds of MHJJ were detected in both positive and negative ion modes (Figure 1A–C), among which 110 active ingredients with a mass spectral similarity score > 0.9 were ranked by mass spectrometry response intensity, as shown in Table 2. The main components screened by UPLC-QE-Orbitrap-MS were

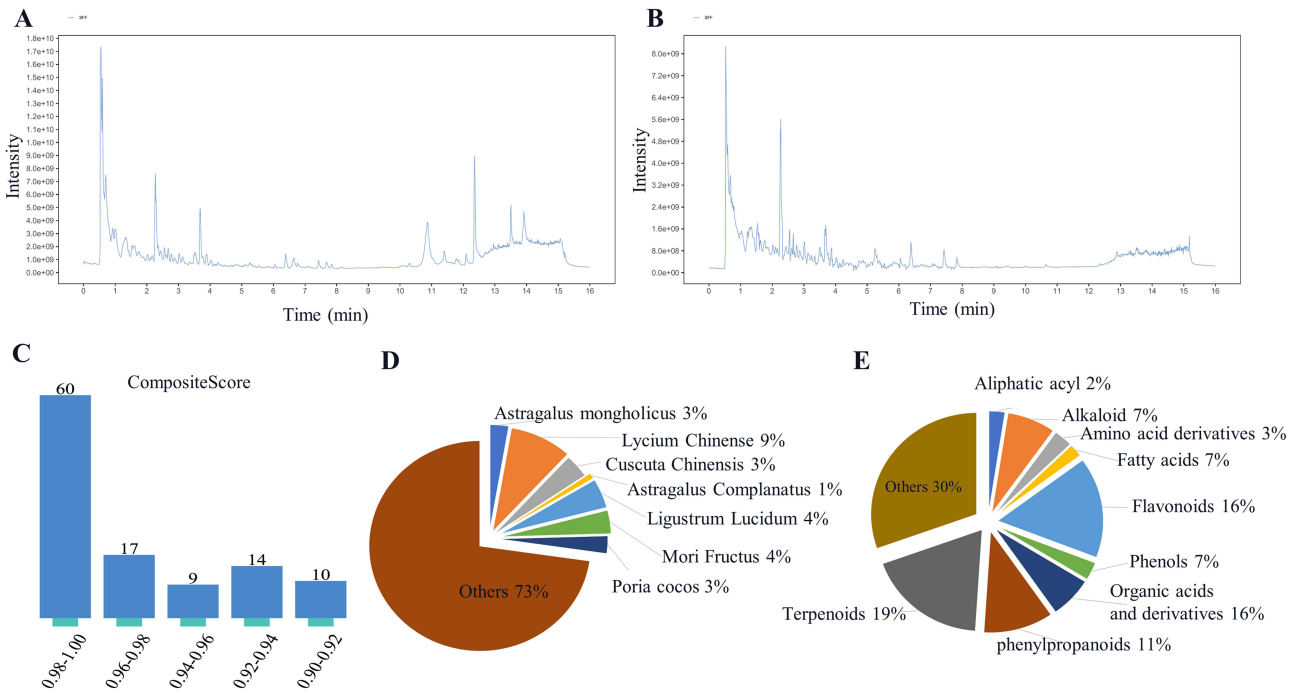

Figure 1 Main components of MHJJ were identified by UPLC-QE-Orbitrap-MS. (**A**) Components were detected in the positive ion mode. (**B**) Components were detected in the negative ion mode. (**C**) Number of active components were identified (spectral similarity scores > 0.9). (**D**) Proportion of the identified components, which are previously identified as characteristic chemicals of several TCMs used in the MHJJ formula. (**E**) Based on the chemical structures, the main chemicals were classified into certain categories.

found to be mainly derived from *Astragalus complanatus, Lycium barbarum, Ligustrum lucidum*, and *Crataegus pinnatifida* (Figure 1D). The components in the MHJJ formula were mainly terpenoids, flavonoids, and alkaloids, as illustrated in Figure 1E.

Table 2 Major Bioactive Components of MHJJ

Molecule	Formula	Classification
Isokobusone	$C_{14}H_{22}O_2$	Sesquiterpenoid
Palmitic acid	$C_{16}H_{32}O_2$	Fatty acid
Kaempferol	$C_{15}H_{10}O_6$	Flavonoid
Oleanolic acid	$C_{30}H_{48}O_3$	Triterpenoid
Curcumenol	$C_{15}H_{22}O_2$	Sesquiterpenoid
p-hydroxybenzaldehyde	$C_7H_6O_2$	Phenol
Daidzein	$C_{15}H_{10}O_4$	Flavonoid
3-phenylpyruvic acid	$C_9H_8O_3$	Phenylpropanoid
2-chloro-dl-phenylalanine	$C_9H_{10}ClNO_2$	Alkaloid
Cuelure	$C_{12}H_{14}O_3$	Others
9-hydroxycalabaxanthone	$C_{24}H_{24}O_6$	Xanthone
1-glyceryl linolenate	$C_{21}H_{36}O_4$	Aliphatic acyl
Diosmetin	$C_{16}H_{12}O_6$	Flavonoid
Dioscorine	$C_{13}H_{19}NO_2$	Alkaloid
Tyramine	$C_8H_{11}NO$	Alkaloid
Ethyl *p*-anisate	$C_{10}H_{12}O_3$	Others
Hispidulin	$C_{16}H_{12}O_6$	Flavonoid
Licoisoflavone A	$C_{20}H_{18}O_6$	Flavonoid
Benzoic acid	$C_7H_6O_2$	Aromatic acid
4-hydroxyphthalide	$C_8H_6O_3$	Phenol

 https://doi.org/10.2147/DDDT.S523809

MHJJ Alleviates CTX-Induced Myelosuppression, Gastrointestinal Disturbances, and Hepatotoxicity

Schematic diagram of the treatment process in mice is shown in Figure 2A. Myelosuppression, gastrointestinal discomfort and hepatic impairment are common adverse effects of CTX. We compared the peripheral blood leukocyte (WBC) and platelets (PLT) counts of each group to characterise the degree of myelosuppression in each group; we recorded body weights on days 21/28/35/49 to characterise differences in nutrient intake due to gastrointestinal discomfort in each group; and we recorded alanine aminotransferase (ALT) and aspartate aminotransferase (AST) levels to compare the degree of liver function impairment in each group. On days 28 and 49, the CTX group showed weight loss compared to the WT group. The MHJJ uninterrupted treatment group showed a dose-dependent increase in body weight compared with the CTX group (Supplementary Figure 1A). On day 49, WBC and PLT appeared decreased in the CTX group compared with the WT group, and WBC and PLT appeared increased after continuous MHJJ intervention, with no difference between MHJJ doses (Supplementary Figure 1B); ALT and AST were abnormally increased in CTX group compared with WT group. Compared with CTX group, ALT and AST in MHJJ group were within the normal range, but there was no difference between different MHJJ doses. (Supplementary Figure 1C).

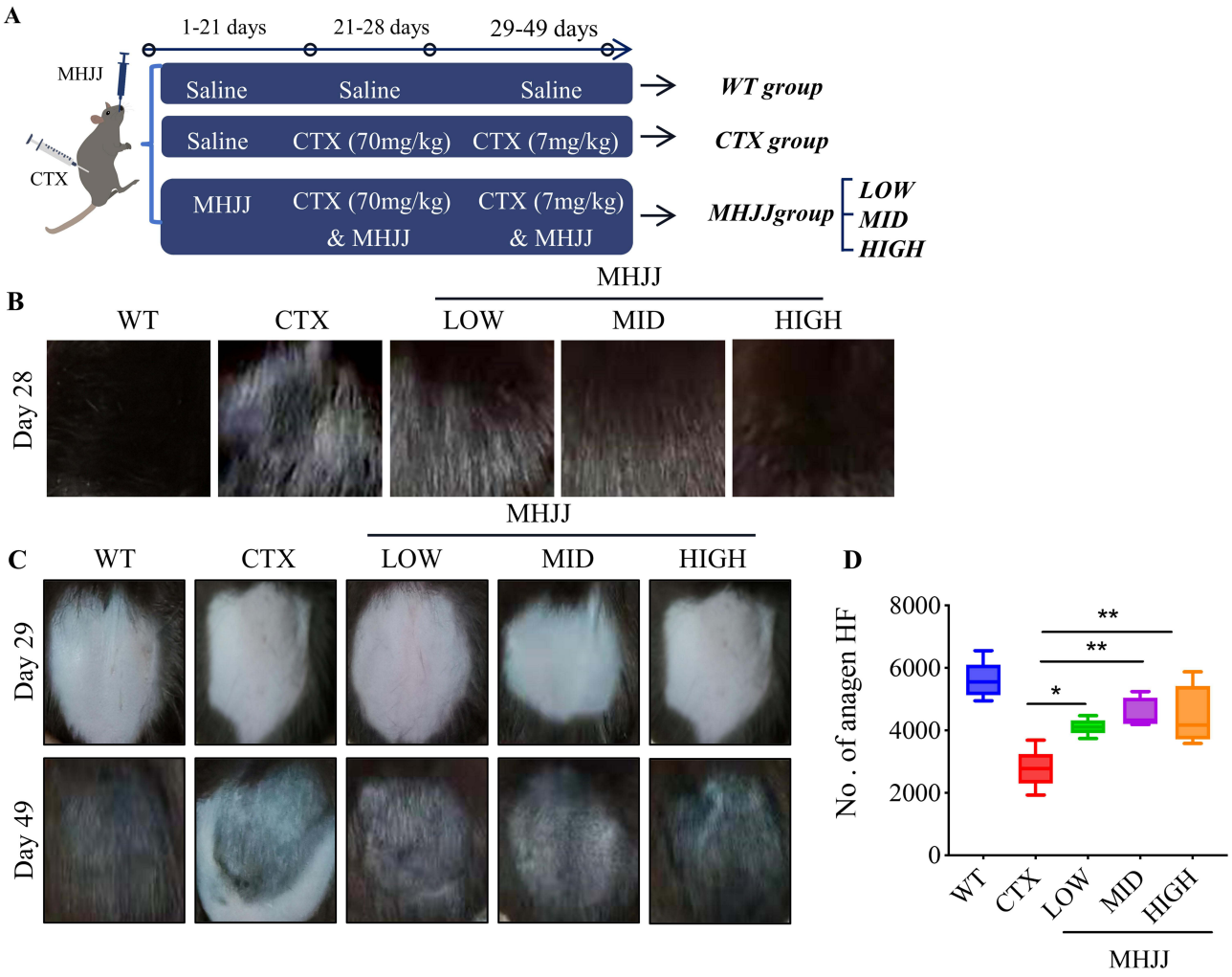

Figure 2 Prevention of CTX-induced alopecia by MHJJ. (**A**) Treatment and observation schedule of mice. (**B**) Alopecia on the back of mice in each group on day 28. (**C** and **D**) Hair regrowth on the back of mice in each group on day 49. (n = 5). Data were presented as mean ± SD. * $P < 0.05$, ** ($P < 0.01$).

https://doi.org/10.2147/DDDT.S523809

MHJJ Prevents CTX-Induced Alopecia and Protects Hair Follicles

On day 28, compared with the black and shiny hair texture of the WT group, hairs in the CTX group were rough and easy to break, and the hair colour became dull and shapeless, which could be shed by light touch, and some of the hairs were actively shedding; the hair shedding in the MHJJ group was significantly reduced, and the hairs in the MHJJ low-dose group were mildly sparse, and the skin could be observed; the hairs in the MHJJ low-dose group were mildly sparse but the skin could not be observed; and the hairs in the MHJJ high-dose group were black, shiny and shiny, and the white skin could not be observed. Dose group had dark and shiny hairs, and no alopecia was observed. Figure 2B shows representative pictures of the hair characteristics of the different treatment groups. In order to clarify the repair effect of MHJJ on damaged hair follicles, next. We treated the back hairs of mice in each group with local depilation and continued to administer the treatment to observe the morphology of the newborn hairs. On day 49, the number of hairs increased in the MHJJ group compared with the CTX group, but there was no difference in the number of hairs between the different doses (Figure 2C and D).

H&E staining of skin tissue sections was performed to observe hair follicle cell structure and growth stages. Images showed that the structure of the hair follicle was restored by the MHJJ treatment. There was a significant increase in the number of melanocytes within the individual follicles of the mice in the MHJJ group, and there was a thickening of the epidermis, with the epidermal muscle tightly attached and the mesenchymal collagen intact (Figure 3A). On day 49, the results of IHC staining of skin tissue sections suggested that the expression of the cell proliferation gene Ki67 was up-regulated in the dorsal skin tissues of the mice in the MHJJ treatment group compared with that of CTX group, the percentage of positive cells for Ki67 in the MHJJ group showed a dose-dependent increase (Figure 3B).

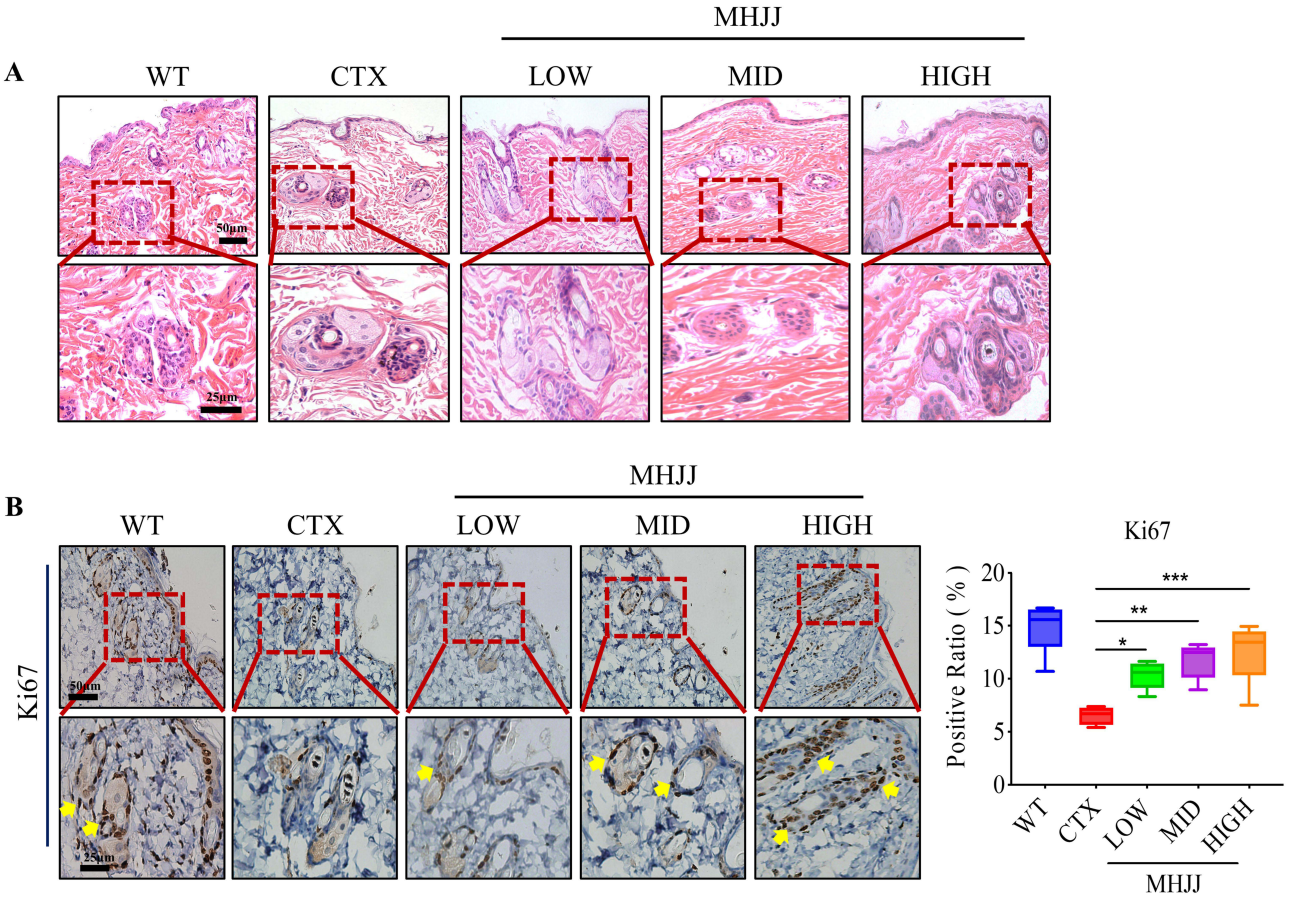

Figure 3 Effects of MHJJ on HFSCs and cell proliferative gene Ki67 in histological skin sections (magnification, 200×; scale bar, 50 μm). (**A**) MHJJ could repair damaged HFSCs in CTX-treated mice. (**B**) Ki67 expressed higher in the dorsal skin of mice after MHJJ treatment (n = 5). Significant differences between the CTX and MHJJ groups were denoted by * ($P < 0.05$), ** ($P < 0.01$), and *** ($P < 0.001$). The yellow arrows indicated the positive staining of Ki67.

The results of tissue immunofluorescence staining indicated that the expression of HFSCs markers Lgr5, CD49f, SOX9, S100A4, CK15 and FZD10 was significantly higher in the MHJJ group than in the CTX group, suggests that MHJJ can significantly promote the activation of HFSCs (Figure 4A). The percentage of positive area of the markers is shown in Figure 4B.

MHJJ Inhibited DNA Hypermethylation Induced by CTX

We used RRBS to analyse the differences in DNA methylation among the WT, CTX and MHJJ groups (MID group) in terms of chromosome-scale levels, GC contents, gene densities and CG/CHG/CHH methylation level. It was found that the DNA methylation levels in the WT and MHJJ groups were slightly lower than those in the CTX group, and were mainly concentrated at the CG level (Figure 5A). Considering the role of the structures of methylated motifs in the identification of DNA-protein binding sites, we identified the methylated site motifs by analyzing the characteristics of the sequences in the upstream and downstream of the methylated cytosines in CG, CHG, and CHH contexts. The results suggested that samples from three groups shared certain commonalities, which were, the motif of CG was CG, the motif of CHG was C (C/A) GG, and the motif of CHH was C (A/C/T) (C/T/A), as shown in Figure 5B. Meanwhile, it was suggested that methylation levels at the same methylated motif sites in the samples from the three groups were basically the same. The methylation modification levels of CHH and CHG motifs were in the 0–0.1% interval, while the ones of CG motifs were in the 0–0.1% and 0.9%–1% intervals (Figure 5C). In addition, the analysis of the methylation of genomic regions revealed that the methylated sites of CHG were upstream2k and downstream 2k and the methylation level in the sample from the CTX group was significantly higher than those from the WT and MHJJ groups. While the

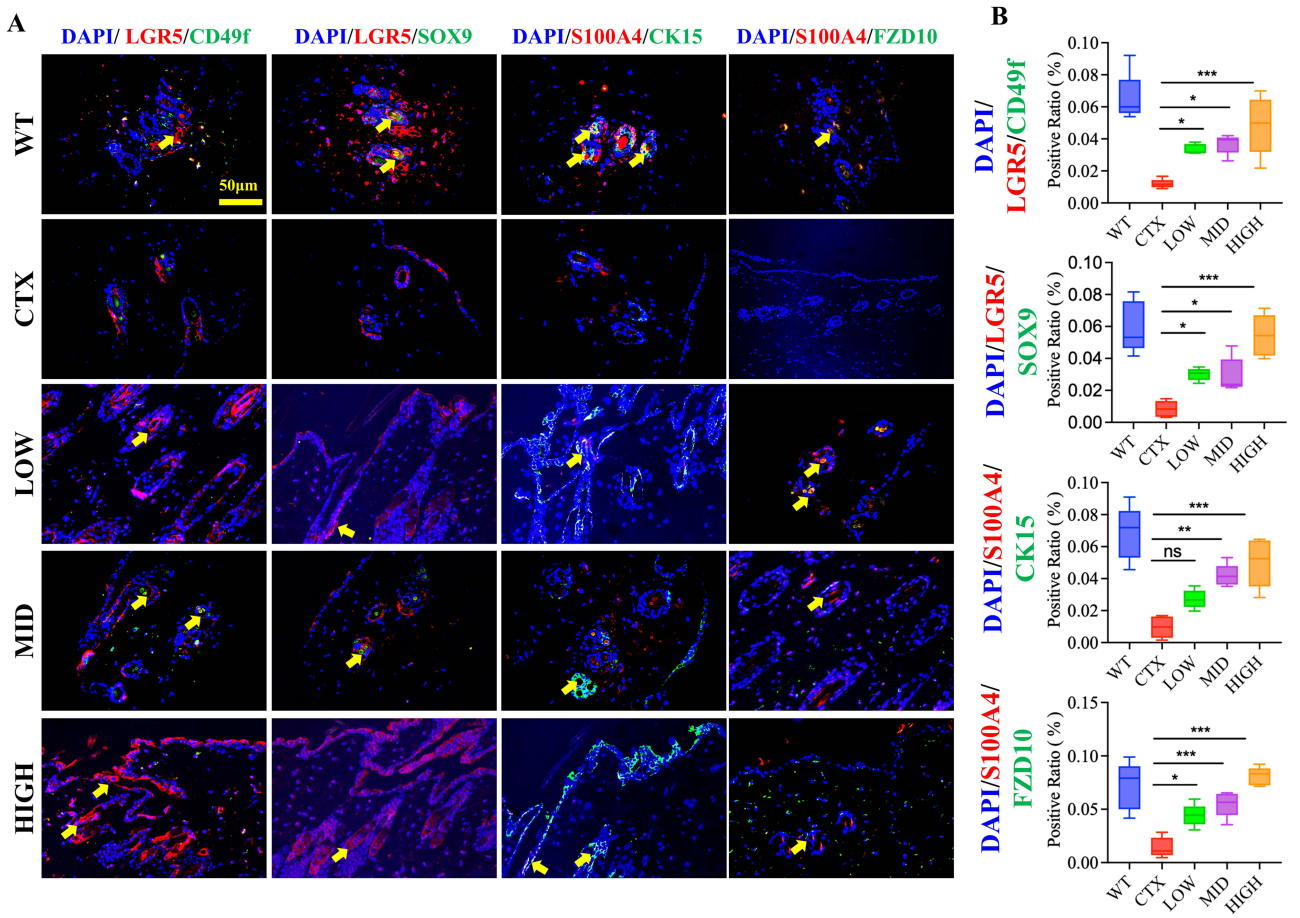

Figure 4 MHJJ promoted the proliferation of HFSCs. (**A**) Representative images of IF-stained HFSCs markers LGR5, CD49f, SOX9, S100A4, CK15, and FZD10 in HFs of dorsal skin tissues (magnification, 200×; scale bar, 50 μm). The yellow arrows indicated the positive staining of HFSCs markers, respectively. (**B**) IF staining positive area ratio (n = 5 per group). Significant differences between the CTX and MHJJ groups were denoted by ^{ns} (not significant), * ($P < 0.05$), ** ($P < 0.01$), *** ($P < 0.001$).

https://doi.org/10.2147/DDDT.S523809

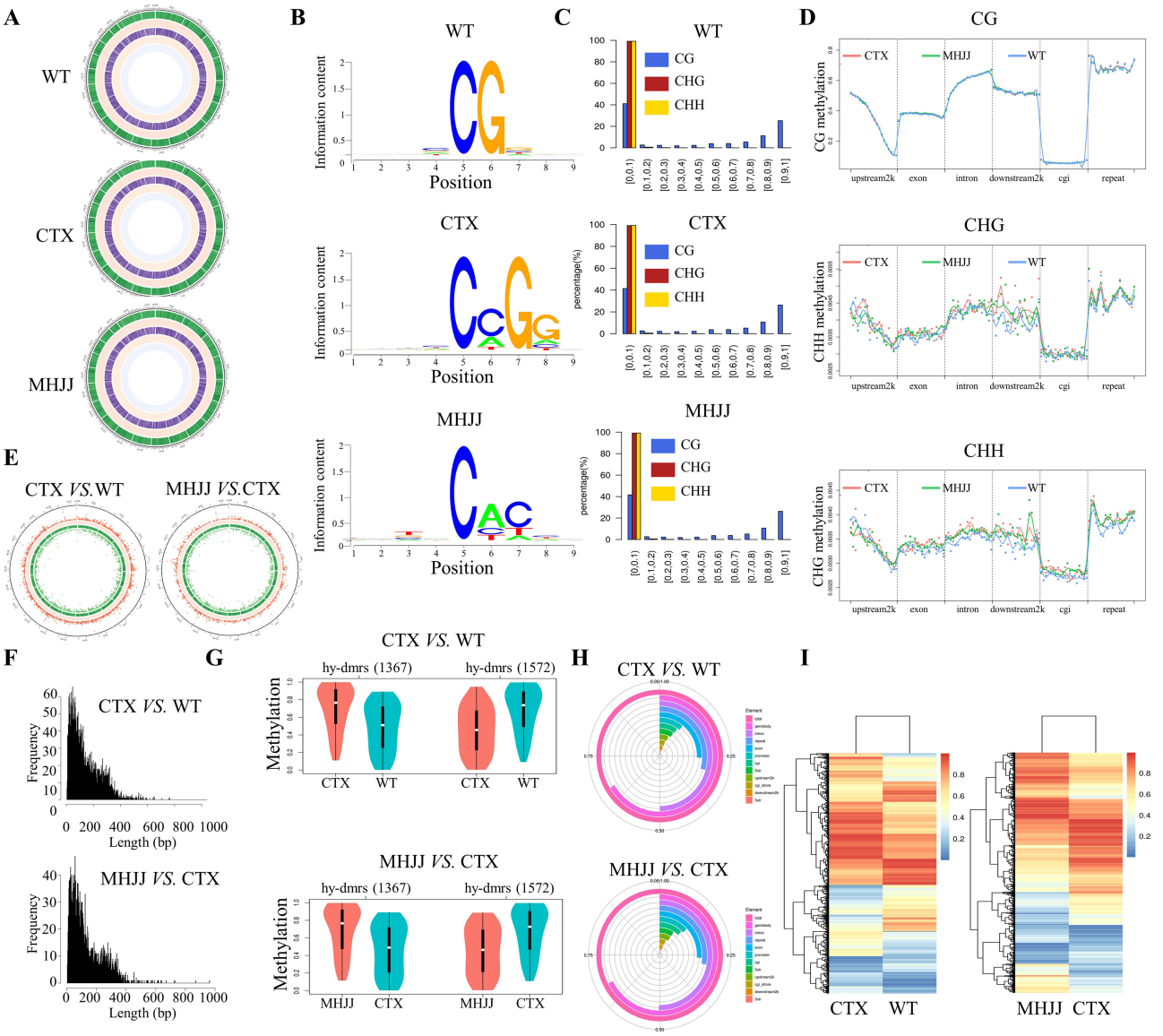

Figure 5 Regulation of differential DNA methylation by MHJJ analyzed by RRBS. (**A**) The Circos plot showed the distribution of methylation levels on the chromosome scale. The outermost circle was the label of the chromosome karyotype, and the five heatmap bars from the outside to the inside in order represented GC content (green), gene density (red), CG methylation level (purple), CHG methylation level (Orange), and CHH methylation level (light blue). Darker colors indicated higher methylation levels. (**B**) The motifs of methylation sites were identified. (**C**) The distribution of methylation levels of cytosine sites was identified. (**D**) The methylation levels of motifs with different methylation sites in genomic functional elements in each group of samples were compared. (**E**) The Circos plot illustrated significant differences in DMRs among the groups. (**F**) The lengths of total DMRs and the lengths of more frequently methylated DMRs. (**G**) The DMR methylation levels in each group. (**H**) Distribution of differential methylation levels of DMRs of genomic regions in each group. (**I**) The Cluster heatmap showed the methylation levels of DMR in each group.

methylated sites of CHH were merely downstream 2k, hypermethylation was observed almost only in the MHJJ group (Figure 5D). The methylation levels in differential methylation regions (DMRs) were further studied. The results showed that higher DMR methylation levels of the CTX group than those of the WT group were observed, and demethylation levels in the MHJJ group were higher than in the CTX group (Figure 5E). The DMRs of samples ranged from 0 to 600 bp in length, and the DMRs with more frequent differential methylation ranged from 0 to 450 bp in length (Figure 5F). According to the analysis of the distribution of DNA methylation levels of DMRs, DMRs in the CTX group were more frequently hypermethylated, while DMRs in the WT group preferred to be hypo- or de-methylated (Figure 5G).

Further studies on the DMRs of genomic regions showed that in the CTX group, the gene body DMR methylation accounted for more than 60% of the total methylation, and the proportions of the intron, repeat, exon, promoter, and CGI DMR methylation was between 15% and 30% methylated compared with the WT group (Figure 5H). As can be seen

from Figure 5I, in terms of WT and CTX groups, a total of 4564 DMR fragments were examined, of which 2483 were hypermethylated (CTX/WT > 3) and 2079 were de- or hypo-methylated (CTX/WT > 3). As for the CTX and MHJJ groups, 2894 DMR fragments were detected, of which 1366 were hypermethylated (MHJJ/CTX > 3) and 1527 were de- or hypo-methylated (MHJJ/CTX > 3).

MHJJ Prevents CTX-Induced Alopecia by Regulating Wnt Signaling Pathway DNA Methylation

We initially confirmed that MHJJ inhibits CTX-induced DNA hypermethylation. To further understand which genes or pathways MHJJ reverses DNA methylation and thus prevents CTX-induced alopecia, we performed co-enrichment analysis of genes that undergo methylation in promoters and gene bodies. In the MHJJ group, the promoter-methylated genes in the BP classification enriched in the "Wnt signaling pathway" classification compared with the CTX group. In terms of the CC classification, and the MHJJ group was more enriched in the "Wnt signalosome and extracellular matrix" (Supplementary Figure 2A). The gene body-methylated genes of the CTX group were in the BP category under the "multicellular organism development and signal transduction" category compared to the WT group, and so was the MHJJ group compared to the CTX group (Supplementary Figure 2B). KEGG pathway analysis revealed that promoter-methylated genes in the MHJJ group compared to the CTX group were mainly located in the Wnt signal transduction pathway (Supplementary Figure 3A). Compared with the MHJJ and WT groups, the gene body-methylated genes were enriched in the Wnt signaling pathway compared to the CTX group (Supplementary Figure 3B).

We validated key genes in the Wnt signaling pathway at the protein level based on the results of suggested methylation sequencing. The expression of Wnt family member 3 (Wnt3) and Wnt family member 10a (Wnt10a) co-stained with LGR5 was significantly lower in the CTX group than in all three MHJJ groups, while the expression of Axin1 and Cerberus 1 (Cer1) proteins co-stained with LGR5 was significantly higher in the CTX group (Figure 6A). The percentage of IF positivity is shown in Figure 6B. These and the sequencing results together indicated the methylation of key genes of Wnt pathway in HFSCs.

MHJJ Modulates Wnt Pathway Genes to Regulate HFSC Proliferation and Apoptosis

Protein expression is regulated both at the transcriptional level (eg DNA methylation occurs in the promoter region of a gene, which inhibits gene transcription and reduces protein expression) and at the post-transcriptional level. We have found that MHJJ can regulate the expression of key proteins in the Wnt pathway and to further understand the mechanism of the drug's efficacy, we examined the transcriptional levels of genes related to proliferation, apoptosis and methylation modification in HFSCs. First, we compared the mRNA expression of proliferation markers in each group based on qRT-PCR experiments. The results showed that mRNA expression of *CD200, KI67, Fzd10, CK15, Lgr5, CD49f, Sox9, S100a4* was down-regulated in the CTX group compared with the WT group; mRNA expression of proliferation-related markers of HFSCs was significantly increased in the MID group compared with the CTX group (Figure 7A). Next, we examined the expression of apoptosis-related genes (*p16, p21* and *p53*) to investigate whether MHJJ has a regulatory role in apoptosis. The transcript levels of cell apoptosis markers were significantly lower in the MID group than in the CTX group, indicating that MHJJ could inhibit the occurrence of apoptosis in HFSCs (Figure 7B).

Significant differences were observed in the expression of DNA methylation and demethylase in WT, CTX, and MHJJ groups, which conforms to the RRBS results (Figure 7C). For the genes in the Wnt signaling pathway, both promoter and gene body were methylated in the intervention groups compared with the CTX group (Figure 7D). The Integrative Genomics Viewer (IGV) analysis showed that Cer1 and Axin1 were hypermethylated in the MID group but hypomethylated in the CTX group. As for Wnt3 and Wnt10a, they were hypomethylated in the promoter and gene body in the MID group but hypermethylated in the CTX group (Figure 7E). A total of four key genes in the Wnt pathway were identified. The qRT-PCR results suggested that in the MHJJ groups, the mRNA expression of *Cer1* and *Axin1* was significantly suppressed than those in the CTX group, while the mRNA of *Wnt3* and *Wnt10a* were significantly higher expressed than those of the CTX group (Figure 7F), This suggests that MHJJ has a potential role in preventing hair loss

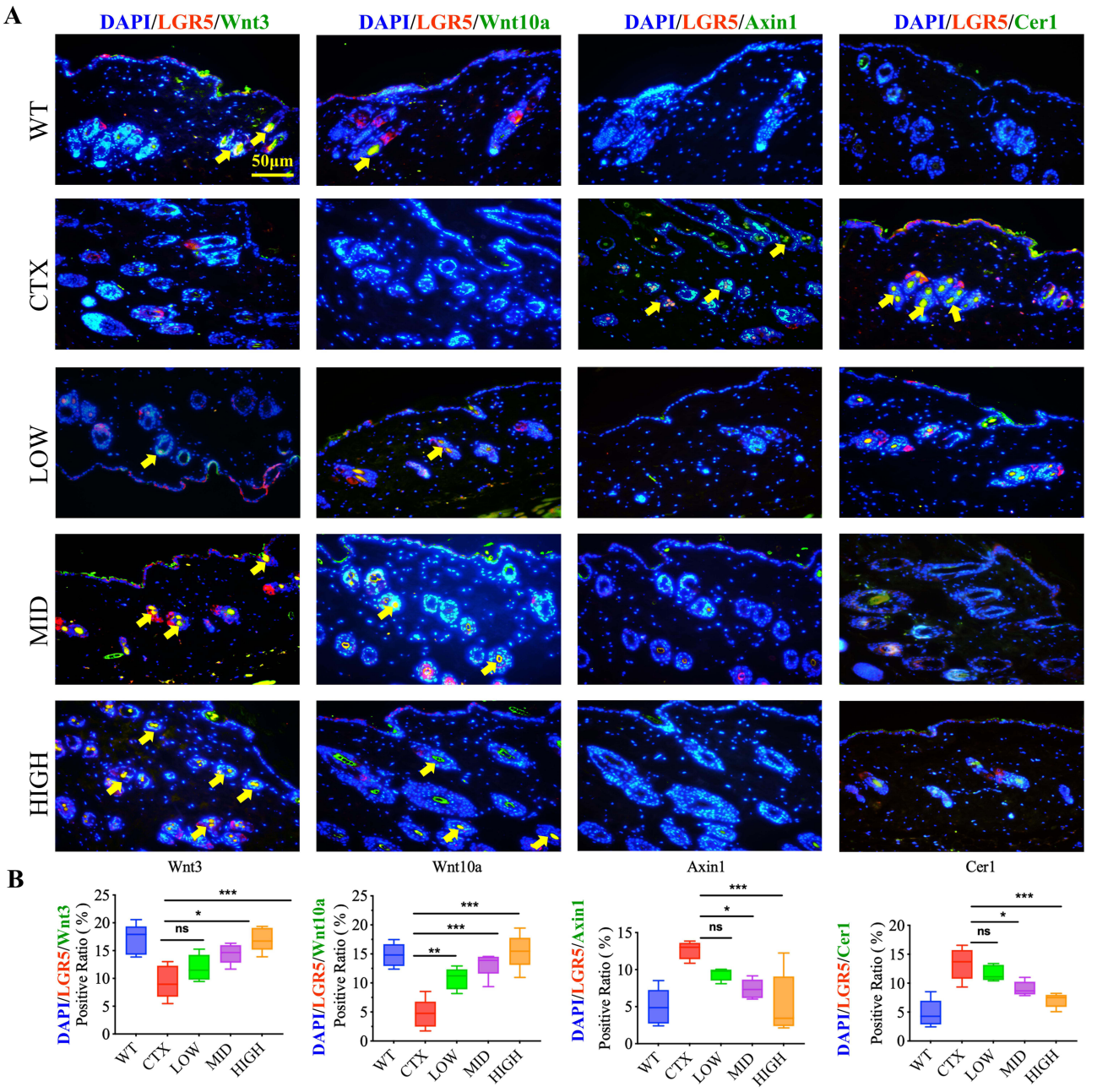

Figure 6 MHJJ regulates methylation modification of Wnt signaling pathway genes affecting the expression of key proteins. (**A**) IF images of co-expression of the HFSCs marker LGR5 and four target genes of the Wnt pathway, Wnt3, Wnt10a, Axin1 and Cer1, in hair follicles of dorsal skin tissue (magnification, 200×; scale bar, 50 μm), and the yellow arrows indicated the positive staining of the HFSCs marker and the Wnt pathway genes, respectively; (**B**) IF staining positive area ratio (n = 5). Significant differences between CTX and MHJJ groups are indicated by ^{ns} (not significant), * ($P < 0.05$), ** ($P < 0.01$) and *** ($P < 0.001$).

and stimulating hair growth by activating the wnt signaling pathway through regulating methylation modification of HFSCs genes.

Discussion

HFSCs have multidirectional differentiation potential and can differentiate into a variety of cell types in the hair follicle, which are the main stem cells for hair generation, and we mainly focused on HFSCs for observation. S100A4 is a member of the S100 family of calcium-binding proteins and can be used as a marker to assist in the localisation of hair follicle stem cells.[38] CD49f is a member of the integrin family, which is primarily used to label hair follicle stem cells.[39]

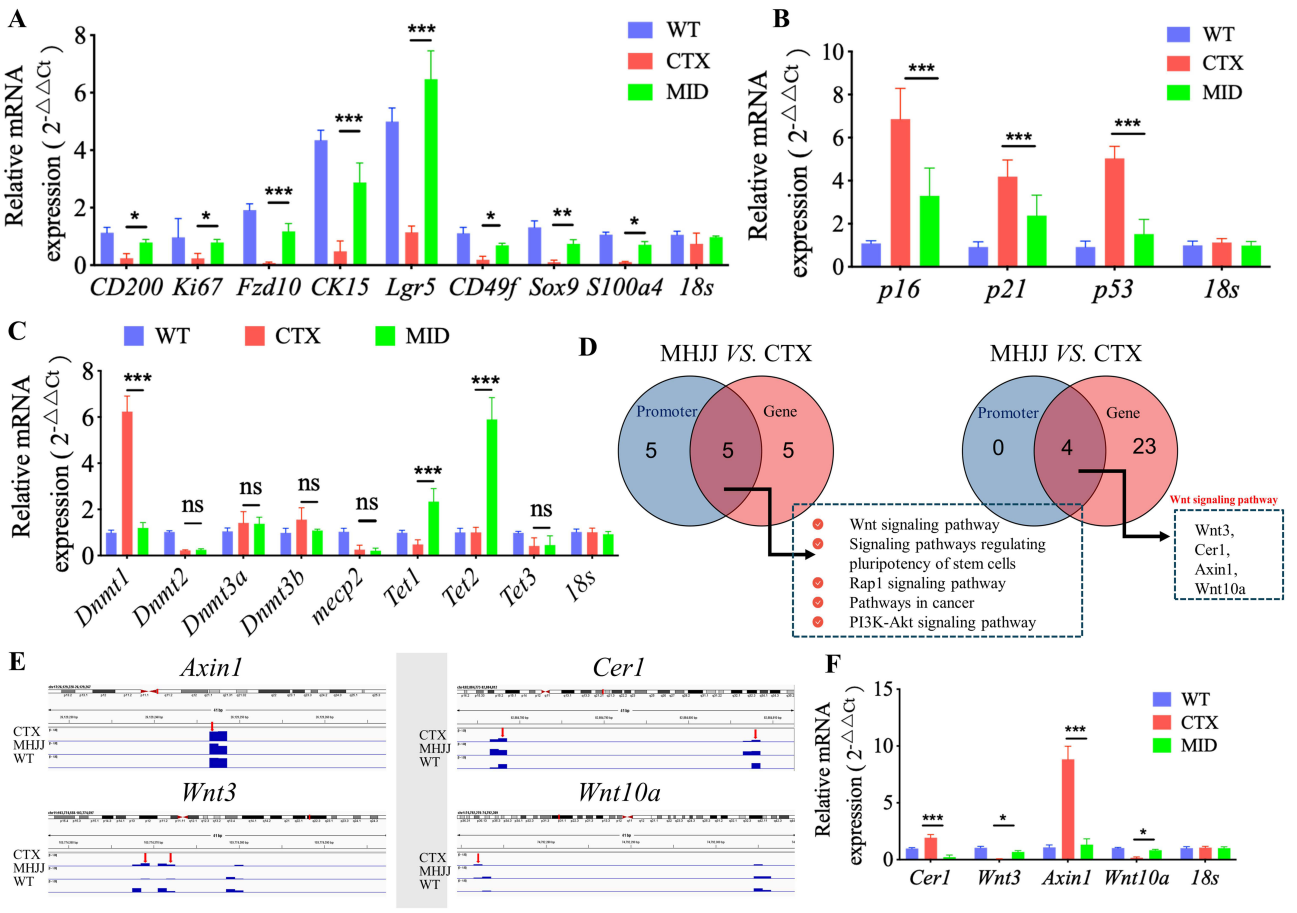

Figure 7 MHJJ regulates proliferation and apoptosis mRNA levels by reducing methylation modification of Wnt signaling pathway genes. (**A**) mRNA expression of proliferation-related markers in HFSCs. (**B**) mRNA expression of cell apoptosis markers. (**C**) mRNA expression of DNA methylesterase and demethylase. (**D**) The left Venn diagram suggested the signal transduction pathways involved in differentially methylated genes in each group, and the right one showed the Wnt pathway genes in which promoter and gene body regions were methylated. (**E**) IGV analysis showed that the key node genes in the Wnt pathway were sequenced, indicating gene methylation was related to the effect of medium dose of MHJJ on treating chemotherapy-induced alopecia in the CTX-induced model. (**F**) The mRNA expression levels of *Cer1, Axin1, Wnt3* and *Wnt10a* were detected by qRT-PCR in the skin tissues of each group. (n = 5). Significant differences were denoted by ^{ns} (not significant), * ($P < 0.05$), ** ($P < 0.01$) and *** ($P < 0.001$).

SOX-9 is an important regulator during neural crest development, in melanocytic differentiation of those adult Nestin+ cells.[40] FZD10 is one of the receptors of the Wnt signaling pathway.[41] When Lgr5 binds to its ligand, it activates a few intracellular signaling pathways, such as the Wnt/β-catenin signaling pathway. Activation of this pathway promotes the proliferation of hair follicle stem cells, allowing them to increase in number while maintaining their stem cell properties.[42] Cer1 is a common target of the WNT signaling pathway in human embryonic stem cells. By directly binding to WNT ligands (eg, WNT3a, WNT8), CER1 inhibits the canonical WNT/β-catenin signaling pathway through blocking their interaction with cell surface receptors such as Frizzled.[43] Axin1 is a key antagonist in the WNT/β-catenin signaling pathway.[44]

Cyclin dependent kinase inhibitor 1A (p21), which inhibits cell cycle protein-dependent kinase (CDK) activity,[45] p21 is a downstream gene of Cellular tumor antigen p53 (p53), and its expression level is regulated by p53.[46] The p21 protein binds to and inhibits the activity of the CDK/cytosolic protein complex, which in turn inhibits Rb phosphorylation that which then blocks the cell cycle. Cyclin dependent kinase inhibitor 2A (p16) is another important cell cycle regulatory protein, which mainly inhibits the activity of cell cycle protein D - CDK4/6 complex and prevents cells from entering S phase from G1 phase, thus achieving the regulation of cell cycle.[47] p16 and p21 block cell cycle progression by inhibiting CDK activity and are directly related to the regulation of the Wnt signaling pathway.[48] In contrast, Bax and

https://doi.org/10.2147/DDDT.S523809

Cleaved Caspase-3 are mainly involved in the execution phase of apoptosis, whereas the present study focuses more on chemotherapy-induced cell cycle arrest rather than direct apoptotic execution.[49]

In carcinogenesis and cancer therapy, the Wnt/β-catenin signaling pathway is a conserved signaling axis participating in diverse physiological processes such as proliferation, differentiation, apoptosis, migration, invasion and tissue homeostasis.[50] A natural compound from the traditional medicinal plant Scutellaria baicalensis, baicalin, was found to promote HF growth through Wnt/β-catenin pathway activation in mouse dermal papillar cells.[51] It was reported that the chemical components of cherry kernel oil promoted hair growth via Wnt/β-catenin signaling pathway.[52] It has been found that DNMT1-mediated methylation suppressed microRNA-214-3p expression and promoted the differentiation of HFSCs into adipocytes.[53] Also, evidence showed that OCT4 can maintain self-renewal by regulating DNA methyltransferase to inhibit p21 to reverse the aging of hair follicle mesenchymal stem cells.[54] These findings suggested that DNA methylation was closely associated with HF damage and repair. It is possible, therefore, that DNA methylation and Wnt/β-catenin pathway might both play critical roles in alopecia. These findings indicate that Wnt signaling pathway mainly involves in the mechanisms of TCMs improving alopecia.

This study first reveals that the traditional Chinese medicine formula MHJJ alleviates cyclophosphamide (CTX)-induced alopecia by epigenetically activating the Wnt signaling pathway in hair follicle stem cells (HFSCs) through dynamic DNA methylation remodeling. The results of MHJJ component analysis shows that this formula's effect of promoting HFs restoration and proliferation is likely to be benefited from its variety of bioactive chemicals. At the molecular level, MHJJ intervention reduces promoter and gene body methylation of Wnt pathway activators (Wnt3, Wnt10a) while increasing methylation of their negative regulators (Cer1, Axin1), thereby potentiating Wnt signaling activity. This epigenetic reprogramming promotes HFSC proliferation (upregulation of Ki67, CD49f) and suppresses apoptosis (downregulation of p21, p16), ultimately driving accelerated hair regrowth and follicular architectural restoration at the organismal level. Due to technical constraints, the current methylation data reflect global epigenetic alterations in skin tissue primarily driven by hair follicle stem cells (HFSCs). Future studies should employ single-cell multi-omics technologies to dissect HFSC-specific regulatory mechanisms at cellular resolution.

Wnt signaling maintains anagen-phase gene expression in vitro and hair inductive activity in skin reconstitution assays.[55,56] Our study shows MHJJ prevents chemotherapy-induced alopecia by inhibiting DNA methylation of Wnt pathway activators, providing new evidence that TCM regulates Wnt signaling to mitigate hair loss. Unlike scalp cooling (which physically blocks drugs from follicles), our research reveals a novel epigenetic mechanism—DNA methylation reprogramming in hair follicle stem cells—for MHJJ's effects.

The demethylation of key genes in HFSCs by MHJJ ultimately showed a decrease in apoptosis and an increase in proliferation of HFSCs. This result is exciting because the theoretical basis of TCM in preventing the side effects of chemotherapy has been further elucidated. However, there are some limitations in this study. For the identification of the main components of MHJJ, UPLC-QEObitrap-MS was used after decoction of the drug, and a more standardised assay would be the mass spectrometry of serum from mice after oral administration of the drug, which is a shortcoming that will be gradually improved by the group in the subsequent experiments. Furthermore, it remains unclear which active components in the MHJJ formula exert the optimal demethylation effect. The activity and content of DNA methylase and demethylase in MHJJ were solely identified at the transcriptome level via PCR, and alterations in protein expression were not detected using Western blot or Elisa methods. Therefore, we will continue to complete this segment of experimental data in subsequent experiments. In addition, this study focuses on the prevention of CTX-induced alopecia by MHJJ, and our team is currently exploring the pharmacodynamic mechanism of MHJJ for the prevention of myelosuppression and gastrointestinal discomfort, which will provide a theoretical basis for the transition of MHJJ as a nosocomial formulation to clinical trials and clinical translation.

Conclusion

MHJJ can prevent chemotherapy-induced alopecia in mice by reducing DNA hypermethylation to activate the Wnt signaling pathway in HFSCs caused by CTX, which provide a basis for further understanding of the therapeutic mechanism of traditional Chinese medicine in chemotherapy-induced alopecia.

Data Sharing Statement

The full complement of data accumulated for these studies is available upon request.

Consent for Publication

Not applicable. All data in this manuscript are available for publication.

Acknowledgment

Xin Liu, Ting Du and Ruofan Xi are co-first authors for this study. We acknowledge the support of Yueyang Hospital of Integrated Traditional Chinese and Western Medicine and Shanghai Geriatric Institute of Chinese Medicine. Yiwen Nie from Yueyang Hospital of Integrated Traditional Chinese and Western Medicine, Shanghai University of Traditional Chinese Medicine is acknowledged for visualization and her comments on the writing and editing of this manuscript during the publication process.

Author Contributions

All authors made a significant contribution to the work reported, whether that is in the conception, study design, execution, acquisition of data, analysis and interpretation, or in all these areas; took part in drafting, revising or critically reviewing the article; gave final approval of the version to be published; have agreed on the journal to which the article has been submitted; and agree to be accountable for all aspects of the work.

Funding

This work was supported by Evidence-Based Capacity Building for TCM Specialty Therapies for Skin Diseases of National Administration of TCM, High-level TCM Key Discipline Construction Project of National Administration of TCM (zyyzdxk-2023065), Integrated Chinese and Western Medicine Diagnosis and Treatment Research Program for Major Difficult Diseases of National Administration of TCM, Cultivation Program of Doctoral Candidates in Key Areas of Shanghai University of TCM (A1-U23-205-03040202), Youth Talent Support Project of the China Society of TCM (2023-QNRC2-B25).

Disclosure

The authors declare that the research was conducted in the absence of any commercial or financial relationships that could be construed as a potential conflict of interest.

References

1. Gumusay O, Renslo JR, Wabl CA, et al. A phase Ib/II study of eribulin with cyclophosphamide (EC) in patients (pts) with advanced breast cancer (ABC). *J Clin Oncol*. 2020;38(15–suppl):e13079–e13079. doi:10.1200/JCO.2020.38.15-suppl.e13079
2. Kim JY, Ohn J, Yoon J-S, et al. Priming mobilization of hair follicle stem cells triggers permanent loss of regeneration after alkylating chemotherapy. *Nat Commun*. 2019;10(1):3694. doi:10.1038/s41467-019-11665-0
3. Farishta M, Deepak V, Parmar M, Winters S. Severe cyclophosphamide-induced pneumonitis in a patient with breast cancer. *Chest*. 2019;156(4):A1506. doi:10.1016/j.chest.2019.08.1333
4. Sikora M, Rudnicka L. Chemotherapy-induced alopecia - the urgent need for treatment options. *J Eur Acad Dermatol Venereol*. 2019;33(2):e69–e70. doi:10.1111/jdv.15207
5. Novice T, Novice M, Shapiro J, Lo Sicco K. Chemotherapy-induced alopecia-A potentially preventable side effect with scalp cooling. *J Am Acad Dermatol*. 2020;82(2):e57–e59. doi:10.1016/j.jaad.2019.09.059
6. Ji Q, Luo Y-Q, Wang W-H, Liu X, Li Q, Su S-B. Research advances in traditional Chinese medicine syndromes in cancer patients. *J Integr Med*. 2016;14(1):12–21. doi:10.1016/S2095-4964(16)60237-6
7. Ni B, Xue K, Wang J, et al. Integrating Chinese medicine into mainstream cancer therapies: a promising future. *Rev Front Oncol*. 2024;14. doi:10.3389/fonc.2024.1412370
8. Zhang M, Liu X, Li J, He L, Tripathy D. Chinese medicinal herbs to treat the side-effects of chemotherapy in breast cancer patients. *Cochrane Database Syst Rev*. 2007;2007(2):Cd004921. doi:10.1002/14651858.CD004921.pub2
9. Tian H, Qin W, Wu W, et al. Effects of traditional Chinese medicine on chemotherapy-induced myelosuppression and febrile neutropenia in breast cancer patients. *Evid Based Complement Alternat Med*. 2015;2015:736197. doi:10.1155/2015/736197
10. Li S, So TH, Tang G, et al. Chinese herbal medicine for reducing chemotherapy-associated side-effects in breast cancer patients: a systematic review and meta-analysis. *Front Oncol*. 2020;10:599073. doi:10.3389/fonc.2020.599073

11. Liu YQ, Wang XL, He DH, Cheng YX. Protection against chemotherapy- and radiotherapy-induced side effects: a review based on the mechanisms and therapeutic opportunities of phytochemicals. *Phytomedicine*. 2021;80:153402. doi:10.1016/j.phymed.2020.153402
12. Zhang QY, Wang FX, Jia KK, Kong LD. Natural product interventions for chemotherapy and radiotherapy-induced side effects. *Front Pharmacol*. 2018;9:1253. doi:10.3389/fphar.2018.01253
13. Tan F, Chen Y, Tan X, Ma Y, Peng Y. Chinese materia medica used in medicinal diets. *J Ethnopharmacol*. 2017;206:40–54. doi:10.1016/j.jep.2017.05.021
14. Wang Y, Sun M, Jin H, et al. Effects of Lycium *barbarum* polysaccharides on immunity and the gut microbiota in cyclophosphamide-induced immunosuppressed mice. *Front Microbiol*. 2021;12:701566. doi:10.3389/fmicb.2021.701566
15. Han J, Fei X, Sun N, Xing J, Cai E, Yang L. Effect of ligustri lucidi fructus on myelosuppression in mice induced by cytoxan. *Biomed Chromatogr*. 2023;37(1):e5524. doi:10.1002/bmc.5524
16. Li J, Niu J, Yang M, et al. Using single-patient (n-of-1) trials to determine effectiveness of traditional Chinese medicine on chemotherapy-induced leukopenia in gastric cancer: a feasibility study. *Ann Transl Med*. 2019;7(6):124. doi:10.21037/atm.2019.02.03
17. Yang DM, Zhang JQ, Fei YF. Lycium barbarum polysaccharide attenuates chemotherapy-induced ovarian injury by reducing oxidative stress. *J Obstet Gynaecol Res*. 2017;43(10):1621–1628. doi:10.1111/jog.13416
18. Shi Y, Leng Y, Liu D, et al. Research advances in protective effects of ursolic acid and oleanolic acid against gastrointestinal diseases. *Am J Chin Med*. 2021;49(2):413–435. doi:10.1142/s0192415x21500191
19. Imran M, Rauf A, Shah ZA, et al. Chemo-preventive and therapeutic effect of the dietary flavonoid kaempferol: a comprehensive review. *Phytother Res*. 2019;33(2):263–275. doi:10.1002/ptr.6227
20. Yuan Q, Zhao L. The mulberry (Morus alba L.) fruit-A review of characteristic components and health benefits. *J Agric Food Chem*. 2017;65(48):10383–10394. doi:10.1021/acs.jafc.7b03614
21. Lee CY, Su CH, Chiang CY, Wu CN, Kuan YH. Observation of the expression of vascular endothelial growth factor and the potential effect of promoting hair growth treated with Chinese herbal BeauTop. *Evid Based Complement Alternat Med*. 2021;2021:6667011. doi:10.1155/2021/6667011
22. Zhou S, Rahman A, Li J, et al. Extraction methods affect the structure of Goji (Lycium barbarum) Polysaccharides. *Molecules*. 2020;25(4):936. doi:10.3390/molecules25040936
23. Zhao Q, Zheng Y, Zhao D, et al. Single-cell profiling reveals a potent role of quercetin in promoting hair regeneration. *Protein Cell*. 2023;14(6):398–415. doi:10.1093/procel/pwac062
24. Liu J, Liu J, Duan S, Liu L, Zhang G, Peng X. Reprogrammed epigenetic landscape-prophesied functions of bioactive polysaccharides in alleviating diseases: a pilot study of DNA methylome remodeling in astragalus polysaccharide (APS)-improved osteoporosis in a rat model. *J Agric Food Chem*. 2020;68(52):15449–15459. doi:10.1021/acs.jafc.0c06483
25. Liu J, Yu J, Peng X. Poria cocos polysaccharides alleviates chronic nonbacterial prostatitis by preventing oxidative stress, regulating hormone production, modifying gut microbiota, and remodeling the DNA methylome. *J Agric Food Chem*. 2020;68(45):12661–12670. doi:10.1021/acs.jafc.0c05943
26. Qiu W, Lin J, Zhu Y, et al. Kaempferol modulates DNA methylation and downregulates DNMT3B in bladder cancer. *Cell Physiol Biochem*. 2017;41(4):1325–1335. doi:10.1159/000464435
27. Cai XM, Zhu BR. [A FAAS analysis of seven elements and a preliminary exploration of their resistance to aging in Huanjingjian oral liquid]. *Zhongguo Zhong Yao Za Zhi*. 1989;14(8):473–5,510. Catalan
28. You X, Xu Y, Huang J, et al. A data mining-based analysis of medication rules in treating bone marrow suppression by kidney-tonifying method. *Evid Based Complement Alternat Med*. 2019;2019:1907848. doi:10.1155/2019/1907848
29. Gibson F, Hanly A, Grbic N, et al. Epigenetic dysregulation in autoimmune and inflammatory skin diseases. *Clin Rev Allergy Immunol*. 2022;63(3):447–471. doi:10.1007/s12016-022-08956-8
30. Lyko F. The DNA methyltransferase family: a versatile toolkit for epigenetic regulation. *Nat Rev Genet*. 2018;19(2):81–92. doi:10.1038/nrg.2017.80
31. Ambrosi C, Manzo M, Baubec T. Dynamics and context-dependent roles of DNA methylation. *J Mol Biol*. 2017;429(10):1459–1475. doi:10.1016/j.jmb.2017.02.008
32. Jeltsch A, Ehrenhofer-Murray A, Jurkowski TP, et al. Mechanism and biological role of Dnmt2 in nucleic acid methylation. *RNA Biol*. 2017;14(9):1108–1123. doi:10.1080/15476286.2016.1191737
33. Cobb JE, Wong NC, Yip LW, et al. Evidence of increased DNA methylation of the androgen receptor gene in occipital hair follicles from men with androgenetic alopecia. *Br J Dermatol*. 2011;165(1):210–213. doi:10.1111/j.1365-2133.2011.10335.x
34. Zhao M, Liang G, Wu X, et al. Abnormal epigenetic modifications in peripheral blood mononuclear cells from patients with alopecia areata. *Br J Dermatol*. 2012;166(2):226–273. doi:10.1111/j.1365-2133.2011.10646.x
35. Sen GL, Reuter JA, Webster DE, Zhu L, Khavari PA. DNMT1 maintains progenitor function in self-renewing somatic tissue. *Nature*. 2010;463(7280):563–567. doi:10.1038/nature08683
36. Li J, Jiang TX, Hughes MW, et al. Progressive alopecia reveals decreasing stem cell activation probability during aging of mice with epidermal deletion of DNA methyltransferase 1. *J Invest Dermatol*. 2012;132(12):2681–2690. doi:10.1038/jid.2012.206
37. Nie X, Geng Z, Liu J, et al. Chinese herbal medicine anticancer cocktail soup activates immune cells to kill colon cancer cells by regulating the gut microbiota-Th17 axis. *Front Pharmacol*. 2022;13:963638. doi:10.3389/fphar.2022.963638
38. Chow KH, Park HJ, George J, et al. S100A4 is a biomarker and regulator of glioma stem cells that is critical for mesenchymal transition in glioblastoma. *Cancer Res*. 2017;77(19):5360–5373. doi:10.1158/0008-5472.Can-17-1294
39. Krebsbach PH, Villa-Diaz LG. The role of integrin α6 (CD49f) in stem cells: more than a conserved biomarker. *Stem Cells Develop*. 2017;26(15):1090–1099. doi:10.1089/scd.2016.0319
40. Stüfchen I, Beyer F, Staebler S, et al. Sox9 regulates melanocytic fate decision of adult hair follicle stem cells. *iScience*. 2023;26(6):106919. doi:10.1016/j.isci.2023.106919
41. Chen X, Shi C, Cao H, et al. The hedgehog and Wnt/β-catenin system machinery mediate myofibroblast differentiation of LR-MSCs in pulmonary fibrogenesis. *Cell Death Dis*. 2018;9(6):639. doi:10.1038/s41419-018-0692-9

42. Sunkara RR, Mehta D, Sarate RM, Waghmare SK. BMP-AKT-GSK3β signaling restores hair follicle stem cells decrease associated with loss of Sfrp1. *Stem Cells*. 2022;40(9):802–817. doi:10.1093/stmcls/sxac041
43. Katoh M, Katoh M. CER1 is a common target of WNT and NODAL signaling pathways in human embryonic stem cells. *Int J Mol Med*. 2006;17 (5):795–799.
44. Qiu L, Sun Y, Ning H, Chen G, Zhao W, Gao Y. The scaffold protein AXIN1: gene ontology, signal network, and physiological function. *Cell Commun Signal*. 2024;22(1):77. doi:10.1186/s12964-024-01482-4
45. Xiong Y, Hannon GJ, Zhang H, Casso D, Kobayashi R, Beach D. p21 is a universal inhibitor of cyclin kinases. *Nature*. 1993;366(6456):701–704. doi:10.1038/366701a0
46. El-Deiry WS, Tokino T, Velculescu VE, et al. WAF1, a potential mediator of p53 tumor suppression. *Cell*. 1993;75(4):817–825. doi:10.1016/0092-8674(93)90500-p
47. Zhang X, Wang J, Tang K, et al. The cell cycle regulator p16 promotes tumor infiltrated CD8+ T cell exhaustion and apoptosis. *Cell Death Dis*. 2024;15(5):339. doi:10.1038/s41419-024-06721-7
48. Davidson G, Niehrs C. Emerging links between CDK cell cycle regulators and Wnt signaling. *Trends Cell Biol*. 2010;20(8):453–460. doi:10.1016/j.tcb.2010.05.002
49. Zhang YF, Su PK, Wang LJ, et al. T-2 toxin induces apoptosis via the Bax-dependent caspase-3 activation in mouse primary Leydig cells. *Toxicol Mech Methods*. 2018;28(1):23–28. doi:10.1080/15376516.2017.1354413
50. Song P, Gao Z, Bao Y, et al. Wnt/β-catenin signaling pathway in carcinogenesis and cancer therapy. *J Hematol Oncol*. 2024;17(1):46. doi:10.1186/s13045-024-01563-4
51. Xing F, Yi WJ, Miao F, Su MY, Lei TC. Baicalin increases hair follicle development by increasing canonical Wnt/β-catenin signaling and activating dermal papillar cells in mice. *Int J Mol Med*. 2018;41(4):2079–2085. doi:10.3892/ijmm.2018.3391
52. Zhou Y, Tang G, Li X, et al. Study on the chemical constituents of nut oil from Prunus mira Koehne and the mechanism of promoting hair growth. *J Ethnopharmacol*. 2020;258:112831. doi:10.1016/j.jep.2020.112831
53. Jin F, Li M, Li X, et al. DNMT1-mediated methylation inhibits microRNA-214-3p and promotes hair follicle stem cell differentiate into adipogenic lineages. *Stem Cell Res Ther*. 2020;11(1):444. doi:10.1186/s13287-020-01864-8
54. Lu Y, Qu H, Qi D, et al. OCT4 maintains self-renewal and reverses senescence in human hair follicle mesenchymal stem cells through the downregulation of p21 by DNA methyltransferases. *Stem Cell Res Ther*. 2019;10(1):28. doi:10.1186/s13287-018-1120-x
55. Kishimoto J, Burgeson RE, Morgan BA. Wnt signaling maintains the hair-inducing activity of the dermal papilla. *Genes Dev*. 2000;14 (10):1181–1185. doi:10.1101/gad.14.10.1181
56. Shimizu H, Morgan BA. Wnt signaling through the β-Catenin pathway is sufficient to maintain, but not restore, anagen-phase characteristics of dermal papilla cells. *J Invest Dermatol*. 2004;122(2):239–245. doi:10.1046/j.0022-202X.2004.22224.x